Journal of Sound and Vibration (2001) **244**(4), 697–716
doi:10.1006/jsvi.2000.3489, available online at http://www.idealibrary.com on IDEAL®

A PROCEDURE FOR THE EVALUATION OF INSTALLED PROPELLER NOISE

R. A. Marretta, G. Davì and A. Milazzo

Department of Mechanics and Aeronautics, University of Palermo, Viale delle Scienze, 90128 Palermo, Italy

G. Lombardi

Department of Aerospace Engineering, University of Pisa, Via Diotisalvi 2, 56126 *Pisa, Italy*

AND

M. Carley

Department of Mechanical and Manufacturing Engineering, Trinity College, Dublin 2, *Ireland*

(*Received* 10 *August* 1999, *and in final form* 15 *November* 2000)

A method for the prediction of the acoustics of a propeller in the flow-field of a wing is presented. The method is used to study the noise generated by the unsteady loading induced on the propeller as it passes through the wing flow-field. Both the aerodynamic and acoustic methods are previously proven techniques, the aerodynamic method being based on a combination of free wake analysis and a three-dimensional boundary element method, while the acoustic calculation is a full-surface, moving medium form of the Ffowcs Williams–Hawkings equation. Calculations are presented for a reference case of a four-bladed low-speed propeller in forward flight. The acoustic predictions are supplemented with retarded time results which relate the radiated noise to the aerodynamic conditions on the blade at the time of noise emission. The noise data and the retarded time results are discussed and related to previous aerodynamic work.

1. INTRODUCTION

One of the main driving forces behind modern aircraft powerplant design is the reduction of noise. While propeller noise has been studied for over 80 years (see the report by Lynam and Webb [1]), it is only with increasingly restrictive noise and environmental regulations that the area has become of central importance in the development of new designs. This has required the development of more accurate models of noise generation. The basis of modern noise calculations lies in the Lighthill equation for aeroacoustics [2] and in the Ffowcs Williams–Hawkings [3] solution for noise generated by solid bodies in arbitrary motion. This formulation in particular has been reformulated in a number of ways for the calculation of propeller and rotor noise, most notably by Farassat [4, 5] in the time domain and Hanson [6] in the frequency domain. While the problem of noise generation by a propeller operating in an axial flow is now quite well understood, the prediction of noise from propellers installed on a wing has not received as much attention. In principle, the prediction requires only the introduction of fluctuating loading and velocity terms on the blade surface but the efficient determination of these terms is the crux of the problem. In this

0022-460X/01/290697 + 20 $35.00/0

paper, we present a technique which integrates an unsteady aerodynamic method (including a wing interference term) with a suitable noise prediction code to examine the effect of wing interference on the noise generated and radiated by the propeller. The problem involves the determination of the aerodynamic source terms (including the time-varying component) and the inclusion of these terms in an acoustic model which makes full use of them. With this as the background, the paper shows the results of a study having two stages: (1) a *free wake analysis* (*FWA*) model to evaluate the aerodynamic characteristics of a tractor propeller [7]; (2) an acoustic calculation including the unsteady blade loading terms from the first stage.

One important effect which has been neglected in this paper is the acoustic effect of the aircraft structure, and in particular the fuselage. The two main factors here are the effect of the fuselage boundary layer and that of scattering from the fuselage surface. The effect of boundary layer refraction is negligible below a flight Mach number of 0·3 making the scattering effect dominant. This effect can be treated analytically for certain simplified problems such as the case of an infinitely long cylinder (as in, e.g., reference [8]), which is used as the basic model of an aeroplane fuselage. Scattering calculations are typically performed by first calculating the acoustic field in the absence of the scattering body, the incident field. In this case, the acoustic field of the propeller(s) would be calculated without including the aircraft proper. The net sound field is then calculated as the sum of the incident field and a scattered field. The requirement is that the net field satisfy some boundary condition on the aircraft surface, the simplest being that the acoustic velocity be zero.

The determination of the scattered field is not a trivial task, especially for the complex geometries typical of modern aircrafts. Boundary integral methods have been developed over the past 10 years which are capable of solving for the field scattered by a general body, a typical example being the work of Gallman *et al.* [9]. The first effect of a rigid surface is to increase the predicted pressure (for an infinite plane, the pressure is doubled) with further effects depending on the exact geometry of the system. A recent paper dealing with the problem of predicting the noise from a twin-engined propeller aircraft uses an integral equation based on the Farassat approach to the acoustics [10, 11]. As is standard, the propeller aerodynamics are calculated without including the effect of the aircraft and the sound field is then predicted by using the calculated aerodynamics. The overall noise is calculated by using this sound field as input to a scattering calculation. The aircraft used in the calculation is not identical to that in this paper but it is similar and the general effects on the field should be comparable. Results presented for the acoustic field of one propeller, with and without the fuselage effect included, show the general trends. The pressure-doubling effect on the side of the fuselage nearest the propeller is as expected and, furthermore, there is a shadow region on the opposite side of the aircraft, with the *SPL* 26 dB less than the maximum. There are also points where, although they do not lie in a direct line of sight from the propeller, the sound level is increased, demonstrating that the effect of the fuselage is not simply to "block" radiation from the propeller.

While none of these scattering effects are taken into account in the method of this paper, they would have to be included in industrial noise predictions. The objective of this paper is to demonstrate an improved method for the first part of the calculation, the prediction of the propeller aerodynamics and incident acoustic field.

2. BACKGROUND OF THE PROBLEM

2.1. AEROACOUSTIC ASPECTS

The prediction of aerodynamically generated noise divides into the estimation of the source characteristics (in terms of known aerodynamic quantities) and the modelling of the

propagation of the generated sound. For propeller noise, the theory for source characterization is that of Ffowcs Williams and Hawkings [3] while the propagation is usually modelled by using the standard methods of linear acoustics. The state-of-the-art is now such that, given sufficient computing power, accurate noise predictions for an isolated propeller are commonplace. The main methods currently available are based on the frequency-domain methods of Hanson [6] and the time-domain techniques of Farassat [4, 5]. In both cases, the formulae are exact, limited only by the accuracy and resolution of the available aerodynamic data. A modern noise prediction scheme such as that described in reference [12] can include propeller incidence, blade vibration and the non-linear terms associated with shock formation. The quality of prediction depends, in the first instance, on the quality of the aerodynamic data available and secondly on the degree to which all of the available information is used. In this paper, a time-resolved aerodynamic method is used to obtain accurate data for an installed propeller; these data are used in an acoustic prediction which takes full advantage of the information available, by including unsteady loading effects. This approach constitutes an improved calculation of the source characteristics by including the time-varying terms as the propeller blade passes through the flow-field generated by the wing and by properly accounting for the noise generated by these time-dependent sources. No account is taken, however, of the effect of the wing on the radiated sound: i.e., no scattering calculation is included.

The accurate calculation of the effect of wing interference on the radiated noise is important. It has been known for some time that unsteady loading is an efficient acoustic source [13] but the difficulty lies in accurately calculating the strength and phase of the loading fluctuations. In this paper, we present a computationally efficient method for such calculations as previously proposed by Carley [14, 15].

2.2. AERODYNAMIC ASPECTS

From a purely aerodynamic point of view, FWA, as confirmed by new experimental results obtained from tests performed on a scale model in the Luminy (France) subsonic wind tunnel [16], is successful in numerically determining wing–propeller interference effects. To date, there have been only a few fundamental experimental studies on wing–propeller interference. One such investigation by Witkowski *et al.* [17] examined the effects of wing–propeller interaction on wing drag by assuming that the flow-field is inviscid and quasisteady behind the propeller. In general, numerical studies of several authors were focussed on the main external factors affecting the performance of an isolated propeller both in tractor and pusher configuration [18–22]. More recently, Yamaguchi and Bose [23] and Bose [24], using a two-dimensional time-domain panel method, have analyzed the behaviour of a propeller in oscillatory motion, as well as under chordwise deflection of large amplitude. Meanwhile, the measurement of helicopter rotor flow in hover has been carried out by Müller *et al.* [25], through a "flow visualization gun" time line technique. When the blade tip speed is low enough so as not to encounter compressibility effects, results show that the results obtained using the quasisteady model are similar to those of the more complex unsteady one. On this basis, the wake and the three-dimensional components of the induced velocity have been investigated and calculated by a hybrid FWA-BEM approach which is shown in detail in references [7] and [26]. In the present work the isolated propeller and the wing in a free stream are modelled by using FWA and BEM respectively, and an algorithm based on the hybrid FWA-BEM approach is applied to find the mutual influence of the wing and propeller and its effects on the generated noise. The inflow conditions to the propeller are affected by the wing and the purpose of the technique

presented here is to use the improved aerodynamic model to enhance the acoustic calculations. Lifting line models have been used for acoustic calculations before this (e.g., Hanson's study of incidence effects [27]) but they have not been applied to the prediction of installation effects.

3. FORMULATION OF THE PROBLEM

Following previous work [7, 28, 29], the free wake analysis and a three-dimensional BEM approach are used to calculate the aerodynamic effects when the wing–propeller system experiences their mutual interference. The complete loading distribution of the propeller is then used in a time-domain formulation for the sound radiated by a solid body moving in a steady uniform flow. The method was previously developed to include arbitrary unsteady loading and is thus capable of making full use of the information provided by the improved aerodynamic method.

3.1. AEROACOUSTIC ASPECTS

The method used for the acoustic calculations of this paper is that of Carley [14, 15] which is a model for the noise generated by a rigid body undergoing arbitrary motion in a uniform flow. The development of the model is summarized here and can be found in more detail in reference [14]. The starting point is the wave equation for a steady, uniform flow,

$$\left(\frac{\mathrm{D}^2}{\mathrm{D}t^2} - c^2\frac{\partial^2}{\partial x_i^2}\right)\rho' = \frac{\mathrm{D}}{\mathrm{D}t}\left[\rho_0 v_n \delta(f)\right] - \frac{\partial}{\partial x_i}\left[l_i\,\delta(f)\right] + \frac{\partial^2 T_{ij}}{\partial x_i \partial x_j}. \tag{1}$$

In this wave equation, the body surface is defined by $f(x) = 0$, with $f < 0$ inside the surface S and $f > 0$ outside S. The surface normal fluid velocity is v_n, the force exerted on the fluid by the blade surface is $\mathbf{l}$ and the tensor $\mathbf{T}_{ij}$ (the Lighthill tensor) is related to the shear stresses in the fluid. The uniform flow velocity (of arbitrary direction) is $\mathbf{U}$, the mean fluid density is ρ_0, the speed of sound c and the flow Mach number $\mathbf{M}_\infty = \mathbf{U}/c$. Here the three source terms are referred to as "thickness", "loading" and "quadrupole" respectively. The first of these is related to the displacement of fluid by the propeller blade and is proportional to $\rho_0 v_n$, the momentum injection at the blade surface, while the loading term is related to the force applied by the blade on the fluid. The third term is only of importance when strong non-linear effects are present and can be neglected for subsonic propellers [30]. Equation (1) can be solved using the Green function given by Garrick and Watkins [31] for acoustic radiation in a uniform flow,

$$G = \frac{\delta(\tau - t + R/(1 - \mathbf{M}_\infty^2)c - \mathbf{M}_\infty \cdot (\mathbf{x} - \mathbf{y})/(1 - \mathbf{M}_\infty^2)c)}{4\pi R}, \tag{2a}$$

$$R = [(1 - \mathbf{M}_\infty^2)(\mathbf{x} - \mathbf{y})^2 + (\mathbf{M}_\infty \cdot (\mathbf{x} - \mathbf{y}))^2]^{1/2}. \tag{2b}$$

The notation of the Green function has been modified to allow an arbitrary inflow direction. The solution of the wave equation is then a convolution of the source terms with the Green function which can be evaluated with the aid of generalized function methods [32] to yield the solution for loading noise p_L in terms of integrals over the blade surface:

$$4\pi p_L' = \frac{1}{c}\int_S \left[\frac{1}{1 - \mathbf{M}_s \cdot \mathbf{D}}\frac{\mathrm{d}}{\mathrm{d}\tau}\left(\frac{\mathbf{l}\cdot\mathbf{D}}{R(1 - \mathbf{M}_s \cdot \mathbf{D})}\right)\right]\mathrm{d}S - \int_S \left[\frac{\mathbf{l}}{R(1 - \mathbf{M}_s \cdot \mathbf{D})} \cdot \left(\frac{\mathbf{R}}{R} - \frac{\dot{\mathbf{R}}}{1 - \mathbf{M}_s \cdot \mathbf{D}}\right)\right]\mathrm{d}S. \tag{3}$$

In this equation, the following terms are defined

$$\mathbf{R} = \partial R/\partial x_i, \qquad \mathbf{D} = \mathbf{R}/(1 - \mathbf{M}_\infty^2) + \mathbf{M}_\infty/(1 - \mathbf{M}_\infty^2), \tag{4, 5a}$$

$$\mathbf{M}_s = \dot{\mathbf{y}}/c, \qquad \mathbf{l} = p\mathbf{n}. \tag{5b, c}$$

Here p is the pressure on the blade and $\dot{\mathbf{y}}$ is the velocity of a point on the blade surface; while in calculating the acoustic integrals all quantities on the blade are evaluated at the retarded time τ, where

$$\tau = t - R/(1 - \mathbf{M}_\infty^2)c + \mathbf{M}_\infty \cdot (\mathbf{x} - \mathbf{y})/(1 - \mathbf{M}_\infty^2)c. \tag{6}$$

Note that in the formulation as presented, no restriction has been placed on the loading or the surface velocity. If unsteady aerodynamic data are available, they can be used in the noise prediction, a point of some importance for a study such as this where unsteady aerodynamic effects are especially relevant.

A numerical code, described in reference [15] has been written to implement the method of equation (3). The necessary input from the aerodynamic code is the time-dependent blade pressure distribution. The unsteady loading is supplied in the form of Fourier series. This method was chosen to allow the derivatives of loading to be calculated with as little numerical noise as possible. It is known [13] that unsteady source terms are acoustically efficient radiators so that the accurate evaluation of the derivatives is of some importance in calculating the radiated noise. The code used for the numerical evaluation of the acoustic integrals, SCRUMPI [15], was developed for the prediction of noise from propellers including the effects of unsteady loading and mean flow. The inputs to the code are a blade mesh and loading distribution along with the operating conditions (flow velocity and direction, propeller rotation speed, etc.). At each time step, the retarded time equation is solved by using a Newton–Raphson method to find τ. The relevant source properties (instantaneous blade loading and radiation direction) are then calculated. Once the required quantities have been evaluated at each mesh point, the acoustic integrals are evaluated by using a trapezoidal rule integration over the blade surface. The only difficulty arises when the blade motion is supersonic but this is not a consideration in this work.

As mentioned above the blade loading is supplied in the form of a Fourier series at each mesh point, to reduce the errors introduced in the numerical differentiation of the on-blade pressure. The coefficients are calculated by fitting a Fourier series to the blade loading as a function of azimuth over one propeller revolution.

3.2. AERODYNAMIC ASPECTS

In order to find the solution of this aerodynamic problem, it is necessary to analyze and model the wake of the propeller blades. In this paper, the FWA approach is first applied to an isolated propeller. This iterative method is based on a convergence criterion imposed on the sheet of vortices leaving each blade to form the propeller wake. The wake sheet is modelled by using the vortex lines starting from the points on the blade [12–14, 33–35].

Following Favier *et al.*, the vortex line radial contraction r_t and axial convection x_t are related to the wake azimuth ψ and are valid in the region near the propeller disk, the so-called *near-wake*; outside a value ψ_s (*far-wake*), the region of flow becomes unstable (see Figure 1). At any rate, the convection dominance of propeller flows like that of interest here makes this essentially irrelevant. The following equation relates the value of ψ_s to J, β, and

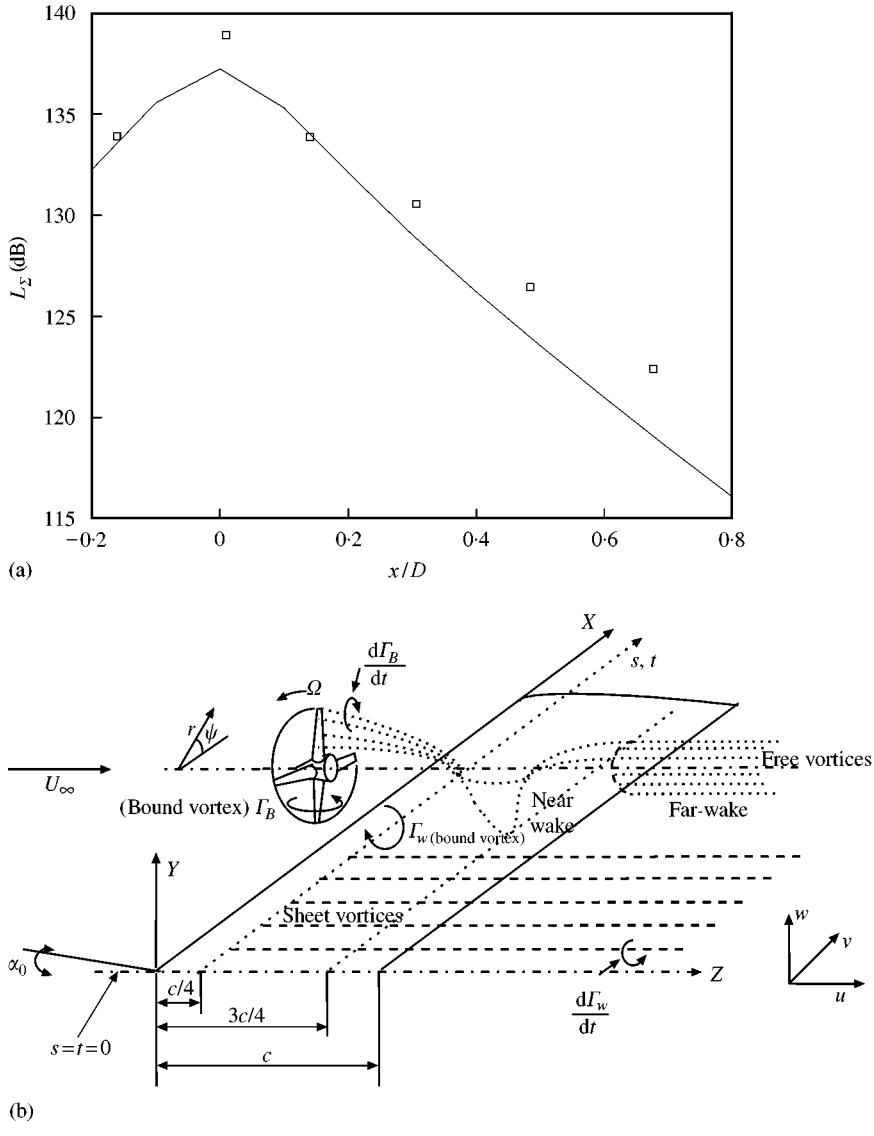

Figure 1. Wing-propeller coupling set-up. (a) Prediction and experimental results for sound pressure level on a sideline for $R = 0{\cdot}6D$. Data from reference [36].

the number of blades B,

$$(\psi_s - \psi_B)/B\psi_B = 0{\cdot}25[8{\cdot}5 - \beta/10 - J(J + 2)], \tag{7}$$

where ψ_B is the angle between each blade, $= 360/B$, J is the advance ratio, and β is the blade angle at $0{\cdot}7R$.

For the tip vortex paths one obtains

$$r_t/R = A + (1 - a)\mathrm{e}^{-\psi/B} \qquad \text{for } 0 \leqslant \psi \leqslant \psi_s, \tag{8}$$

$$x_t/R = K_1(\psi/\psi_B) \qquad \text{for } 0 \leqslant \psi \leqslant \psi_B, \tag{9}$$

$$x_t/R = K_1 + K_2(\psi/\psi_B - 1) \qquad \text{for } \psi_B \leqslant \psi \leqslant \psi_s, \tag{10}$$

where a is an experimentally determined constant, and A, K_1, and K_2 are related to β and J. By similarity the relationship between the inner vortex line radial contraction r_v and the tip vortex contraction is

$$r_v/R = \xi r_t(\psi) \quad \text{for } 0 \leqslant \psi \leqslant \psi_s \tag{11}$$

and for the inner vortex line convection, x_v, one obtains

$$x_v/R = H(r, 0)\psi \quad \text{for } 0 \leqslant \psi \leqslant \psi_B, \tag{12}$$

$$x_v/R = H(r, 0)\psi_B + H(r, \psi_B)(\psi - \psi_B) \quad \text{for } \psi_B \leqslant \psi \leqslant \psi_s, \tag{13}$$

where the functions $H(r, 0)$ and $H(r, \psi)$ depend on the co-ordinates of the vortex filament (ψ, ψ_B).

The velocities u, v, w induced by the wing and its wake at any point on the blade, P, may be obtained by relating the wing lift coefficient, C_L, to the wing and wake vortex strengths and by using the Kutta–Joukowski theorem. H may then be found as a function of the induced velocity components u, v, and w, and ψ:

$$H(u, v, w, \psi, r) = \left(\frac{\pi}{180}\right)(U_\infty + u)\xi/[\Omega r + v\cos\psi - w\sin\psi]. \tag{14}$$

It should be noted that the induced velocity, is given by equation (15) below. Through the Biot–Savart law, applied to the blade circulation $\Gamma(\xi)$, and to the trailing wake vortices, one obtains the induced velocity at any point in the wake as follows:

$$\mathbf{V}_P = \frac{1}{4\pi}\int_{R_0}^{R} \Gamma(\xi)\frac{\mathrm{d}\mathbf{l}\times\mathbf{r}}{|\mathbf{r}|^3} + \frac{1}{4\pi}\int_{\xi_0}^{l}\left[\frac{-\,\mathrm{d}\Gamma(\xi)}{\mathrm{d}\xi}\int_{L(\xi)}\frac{\mathrm{d}\mathbf{l}\times\mathbf{r}}{|\mathbf{r}|^3}\right]\mathrm{d}\xi \tag{15}$$

In equation (15), $\mathbf{r}$ represents the position vector of a space point P with respect to the vortex coordinate system, $L(\xi)$ is the vortex filament leaving the point ξ of the blade, and $\mathrm{d}\mathbf{l}$ is the vector parallel to the direction of the bound vortex in the first integral, and to the trailing vortex filaments in the second one. By noting that the bound vortices never influence the *near-wake* region, one can assume this influence to be small and $\mathrm{d}\mathbf{l}\times\mathbf{r}$ vanishes. After having determined the circulation, Γ, from equation (15) the velocity induced at the point P by the sheet vortices may be written as a superposition, on each blade, of the integrals

$$\mathbf{V}_{ia}(P) = \frac{1}{4\pi}\sum_{p=1}^{B}\int_{\xi_0}^{l}\Gamma(\xi)\frac{\boldsymbol{\tau}_p\times\mathbf{r}_p}{|\mathbf{r}_p|^3}\,\mathrm{d}\xi, \tag{16}$$

where $\boldsymbol{\tau}_p$ is the vector parallel to the direction of the sheet vortex filament. Therefore, the velocity $\mathbf{V}_{il}$ induced by the free vortices at point P may be written as

$$\mathbf{V}_{il}(P) = \frac{1}{4\pi}\int_{R_0}^{R}\frac{\mathrm{d}\Gamma(\xi)}{\mathrm{d}\xi}\,\mathbf{G}(P, \xi)\,\mathrm{d}\xi, \tag{17}$$

where the influence coefficients $\mathbf{G}(P, \xi)$ are expressed as

$$\mathbf{G}(P, \xi) = -\int_{Lp(\xi)}\sum_{p=1}^{B}\frac{\boldsymbol{\tau}_p\times\mathbf{r}_p}{|\mathbf{r}_p|^3}\,\mathrm{d}\mathbf{l}. \tag{18}$$

As regards the model development of the *far-wake* regions, this can be found in reference [28]. Meanwhile, the strength to assign to the vortices of the far-wake is that of the last vortices of the near-wake.

4. RESULTS AND DISCUSSIONS

An initial test was performed to check the results generated by the method against the experimental data of Šulc *et al.* [36]. In this paper, results were presented for the noise generated by a three-bladed wing-mounted propeller in flight. A calculation was performed for the operating conditions of Figure 5(a) of reference [36] and the comparison is shown in Figure 1(a). Since the microphones used in the test were flush-mounted in the aircraft fuselage, 6 dB has been added to the predictions to account for the pressure-doubling effect of the surface. As can be seen the predictions match the experimental data quite well.

As a more detailed example of applying the method, a rectangular wing of aspect ratio, $AR = 6{\cdot}6$ is considered. The wing has a RA1843N1L1 airfoil [16] and negligible dihedral angle. The propeller has a diameter $2R = 0{\cdot}833$ of the wing chord c, having four blades of constant NACA 64A408 airfoil section. The operating conditions are those of Chiaramonte *et al.* [16]: i.e., the propeller advance ratio equals 0·89, the blade pitch β varies from 23 to 32°, the freestream velocity is 17·2 m/s, rotational frequency 1360 rpm and the wing angle of attack is 0°. The simulation technique permits positioning of the propeller anywhere along the wingspan and, to check the experimental results, it was positioned near the wing tip with a distance between the propeller disk and the wing leading edge of $0{\cdot}25c$. The comparison between the aerodynamic results obtained with the present hybrid technique against the data of Chiaramonte *et al.* [16] is shown in reference [7]. Here, only the resulting acoustic predictions are shown.

Results from the farfield calculations are shown in Figures 2–5. We concentrate initially on the $\beta = 23°$ predictions, Figures 2 and 3. Figure 2 shows the predicted first harmonic strength on a sideline extending 5 blade radii up and downstream of the propeller at an

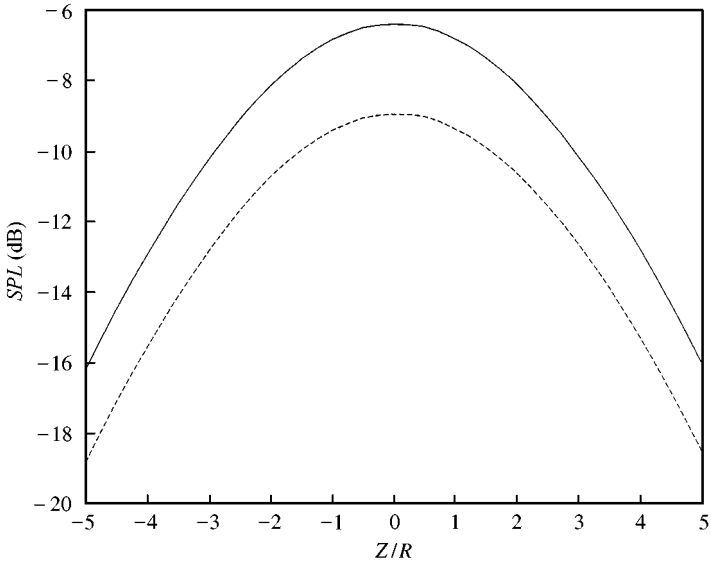

Figure 2. (far field). First harmonic directivity against Z, $r/R = 10$, $\theta = 0$, $\beta = 23°$, isolated (solid) and installed (dashed) propeller.

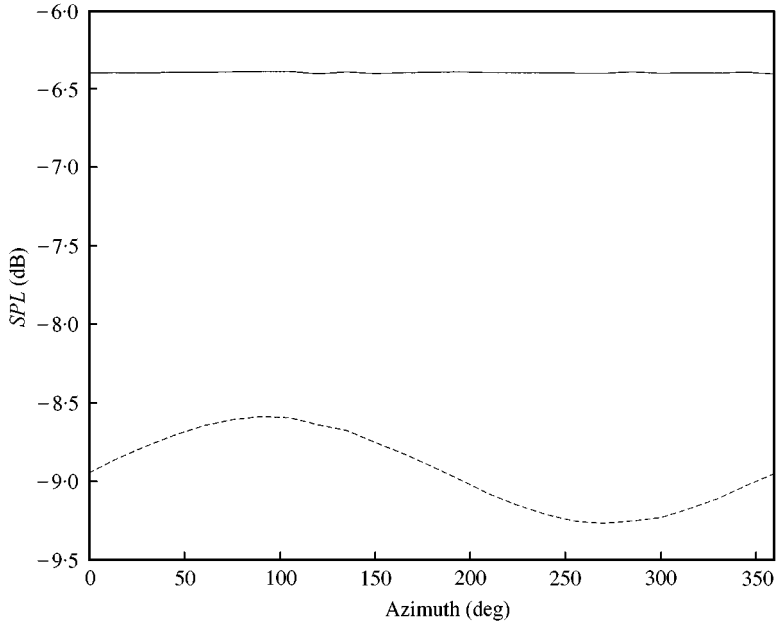

Figure 3. (far field). First harmonic directivity against θ, $Z/R = 0$, $r/R = 10$, $\beta = 23^\circ$, isolated (solid) and installed (dashed) propeller.

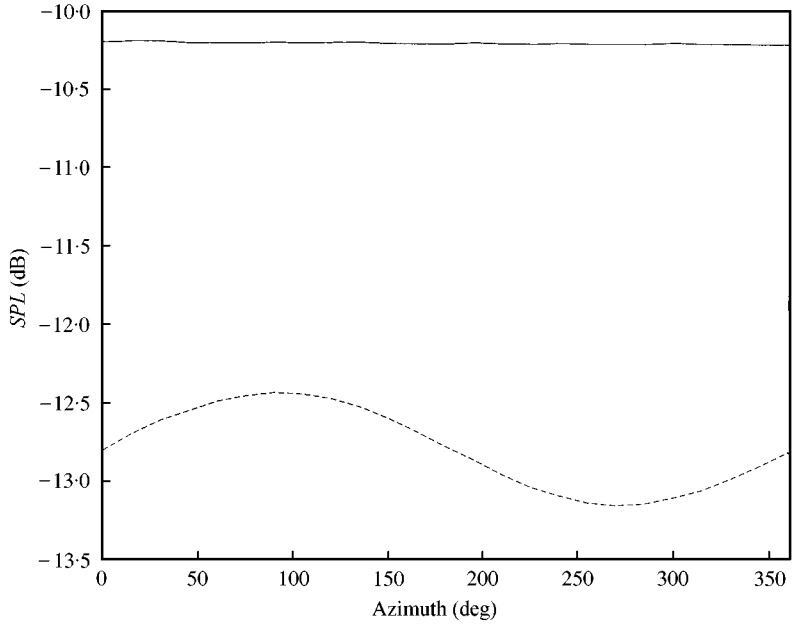

Figure 4. (far field). First harmonic directivity against θ, $Z/R = -3$, $r/R = 10$, $\beta = 23^\circ$, isolated (solid) and installed (dashed) propeller.

azimuth $\theta = 0^\circ$. As expected, the directivity patterns are very similar but the installed propeller acoustic power is about 2·5 dB lower than in the isolated case. This difference is a function of azimuth and can be seen more clearly in Figures 3–5 which show the predicted

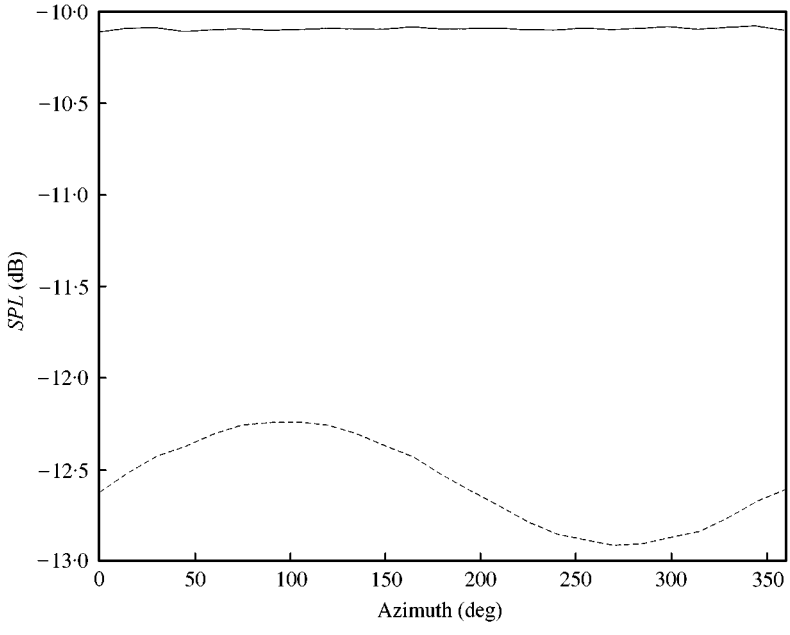

Figure 5. (far field). First harmonic directivity against θ, $Z/R = 3$, $r/R = 10$, $\beta = 23^\circ$, isolated (solid) and installed (dashed) propeller.

first harmonic strength as a function of azimuth in the propeller plane and at 3 blade radii up and downstream of the propeller. There is an obvious variation in the installed propeller first harmonic, due to the variation in loading, but it remains about 2·5 dB below the isolated propeller level at each of the axial stations.

Turning to the nearfield data for $\beta = 23^\circ$, Figures 6–9, one can see similar trends to those in the far field case though, naturally, with higher sound pressure levels. Figure 6 shows the directivity on a sideline at a distance $r/R = 2$, extending 5 blade radii up and downstream of the propeller plane. The directivity patterns are similar in each case with the installed propeller noise about 2 dB lower than that in the isolated case. The azimuthal variation of the loading noise at three axial stations is shown in Figures 7–9, for $z/R = 0, -3, 3$. The variation of the installed propeller noise with azimuth is quite weak in this case being strongest at $z/R = -3$, varying by almost 1 dB, and weakest in the propeller plane.

For the other two blade pitches considered, the trends are quite similar but the levels change. The installed propeller data are practically identical, a point which we discuss later, but in the isolated propeller case, the change in *SPL* is large. Figure 10 compares the isolated propeller, farfield noise for $\beta = 27^\circ$ at $r/R = 10$, to the reference case $\beta = 23^\circ$. Figure 11 shows the same comparison for $\beta = 32^\circ$. The effect of changing the pitch from 23 to 27° is to add about 2 dB to the first harmonic noise level while the change to 32° adds another 2 dB to the radiated noise. This does not occur in the installed propeller case where the curves are indistinguishable. This suggests that the acoustic effect of the change in blade pitch is swamped by the effect of the wing flow field, at least to the approximations used here.

Finally, we show the change in nearfield noise for the isolated propeller in Figures 12 and 13, the installed propeller directivities being practically identical. The effect of the change of the pitch is most noticeable downstream of the propeller, where the $\beta = 27^\circ$ level is 2–3 dB higher than the $\beta = 23^\circ$ result. Upstream of the propeller, the increase is between 1 and

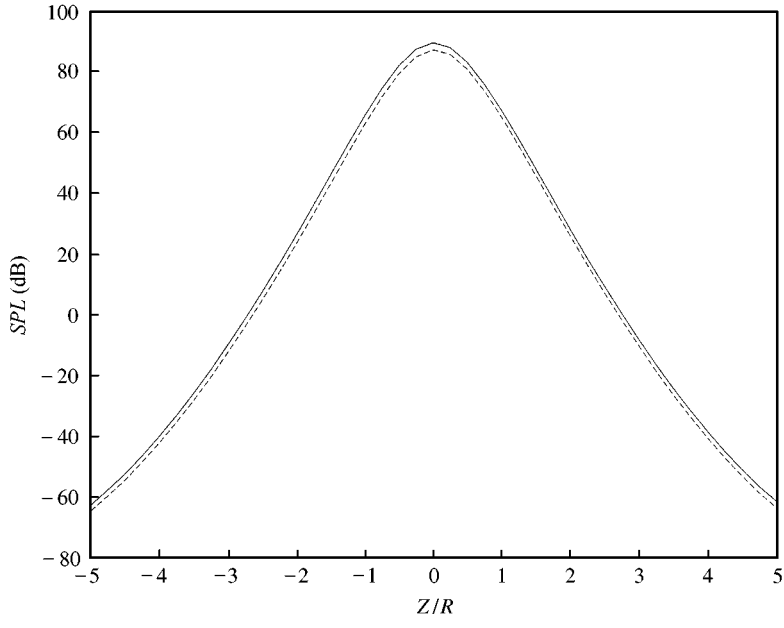

Figure 6. (near field). First harmonic directivity against Z, $r/R = 2$, $\theta = 0$, $\beta = 23^\circ$, isolated (solid) and installed (dashed) propeller.

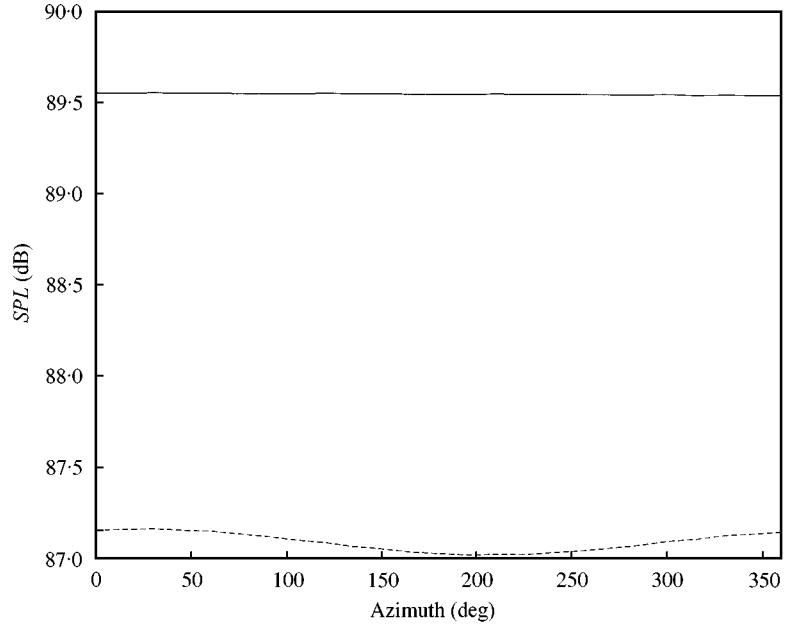

Figure 7. (near field). First harmonic directivity against θ, $Z/R = 0$, $r/R = 2$, $\beta = 23^\circ$, isolated (solid) and installed (dashed) propeller.

2 dB. Comparing the $\beta = 32$ and 23° data, Figure 13, shows that the effect of the increase in pitch is to add up to 5–7 dB to the noise downstream of the propeller and 2–4 dB in the upstream direction.

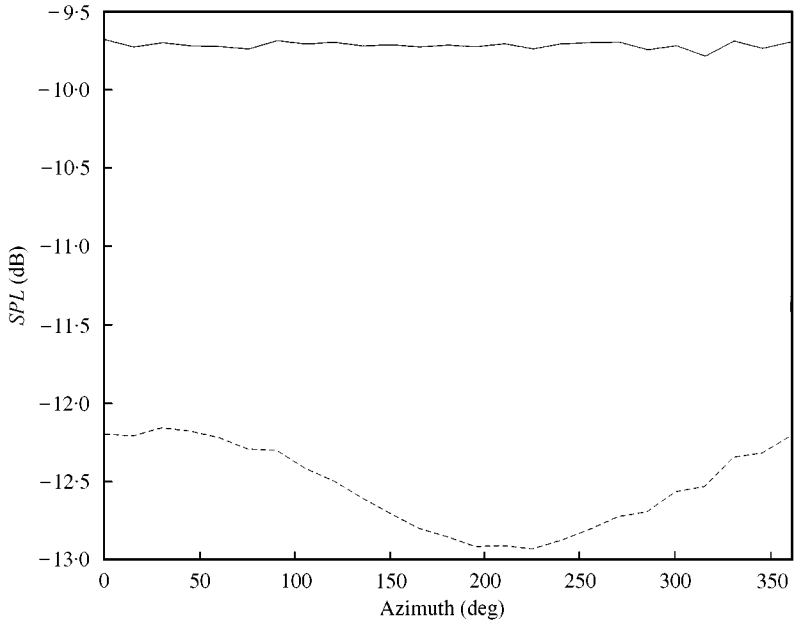

Figure 8. (near field). First harmonic directivity against θ, $Z/R = -3$, $r/R = 2$, $\beta = 23^\circ$, isolated (solid) and installed (dashed) propeller.

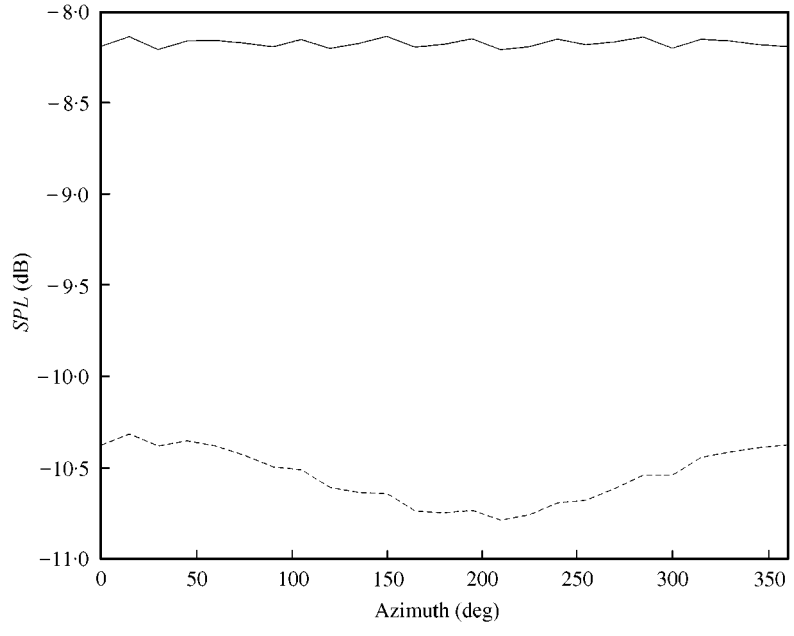

Figure 9. (near field). First harmonic directivity against θ, $Z/R = 3$, $r/R = 2$, $\beta = 23^\circ$, isolated (solid) and installed (dashed) propeller.

Overall, the results seem to indicate that changes in blade pitch are important only for the installed propeller, possibly because the blade loading in the installed case is dominated by the effect of the wing.

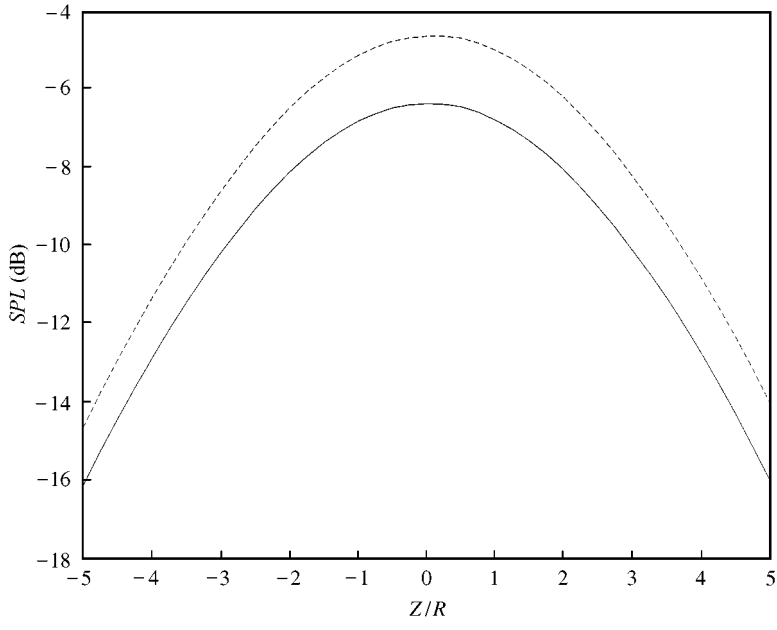

Figure 10. (far field). First harmonic directivity against Z, $r/R = 10$, $\theta = 0$, $\beta = 23^\circ$ (solid), $\beta = 27^\circ$ (dashed).

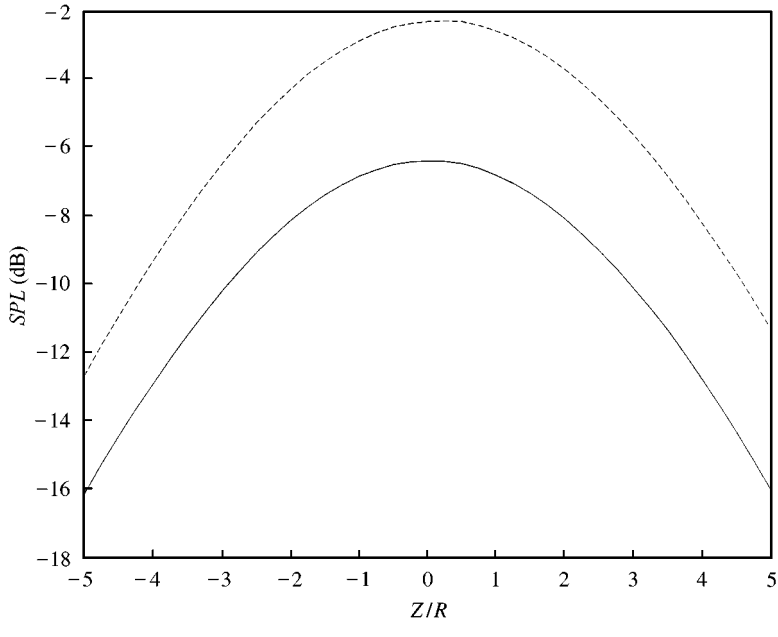

Figure 11. (far field). First harmonic directivity against Z, $r/R = 10$, $\theta = 0$, $\beta = 23^\circ$ (solid), $\beta = 32^\circ$ (dashed).

4.1. RETARDED POSITION PLOTS

To clarify the effect of wing interference and the associated unsteady loading on the noise radiated by the propeller, data are presented as a function of the emission time. The time

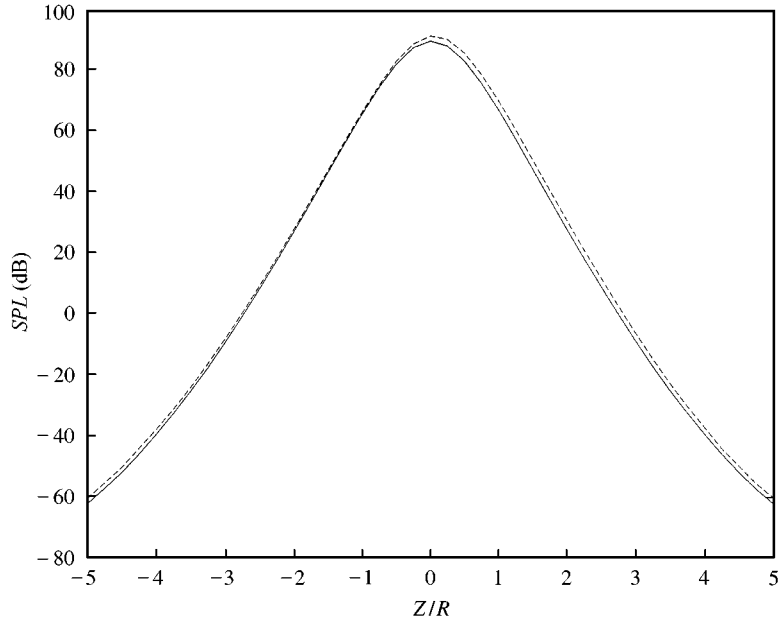

Figure 12. (near field). First harmonic directivity against Z, $r/R = 2$, $\theta = 0$, $\beta = 23^\circ$ (solid), $\beta = 27^\circ$ (dashed).

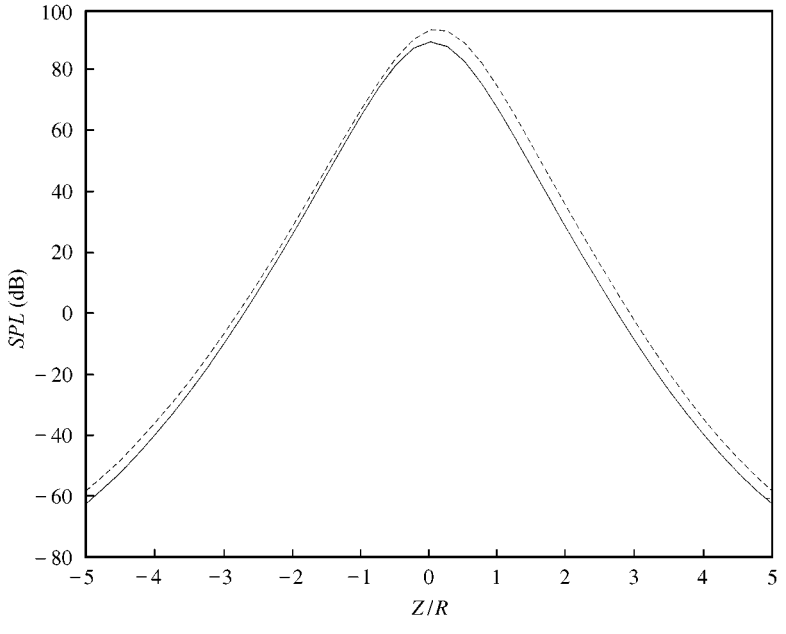

Figure 13. (near field). First harmonic directivity against Z, $r/R = 2$, $\theta = 0$, $\beta = 23^\circ$ (solid), $\beta = 32^\circ$ (dashed).

record of the noise radiated by a single blade is shown as a function of the azimuthal position of the blade tip at the time of emission of the noise received by the observer. This allows the radiated noise to be linked to the unsteady loading on the blade. Figure 14 shows such data for the nearfield noise radiated by the blade at 23° pitch. For comparison, the

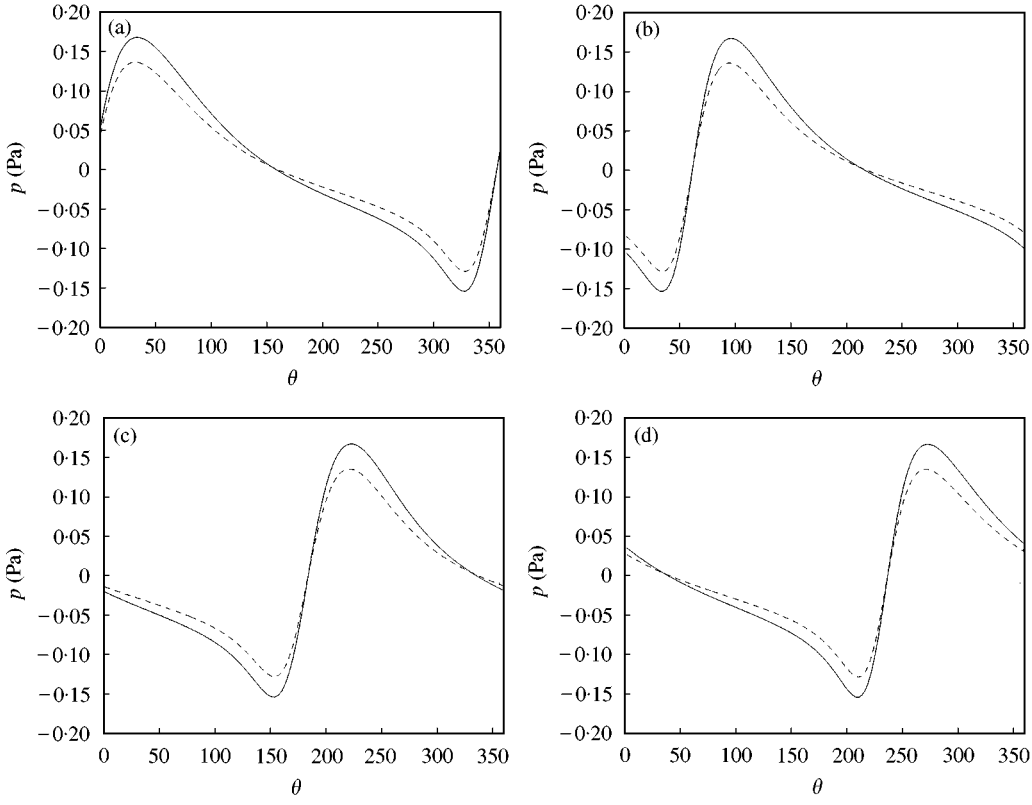

Figure 14. Near field time records as a function of blade tip azimuth at emission time, isolated (solid) and installed (dashed) propeller. (a) 0° observer position; (b) 90° observer position; (c) 180° observer position; (d) 270° observer position.

isolated propeller signal is shown as a solid line, the installed propeller noise being shown dashed. The unsteady component of loading at a point near the blade tip is shown in Figure 15. In Figure 14, all time records show the noise in the propeller plane two blade radii from the propeller axis. In the case of an isolated propeller, all of the time records are identical but with a phase shift dependent on the azimuthal position of the observer. For the isolated propeller, the altered mean loading is responsible for differences between the installed and uninstalled time records, and also for differences between the time records for observers at different azimuthal positions. This difference is shown in Figure 16 for four observer positions, 0°, 90°, 180° and 270°, in the propeller plane. The reference position is 0° and the other time records have been phase shifted by the appropriate amount to facilitate comparison. Again, data are plotted against blade tip azimuthal position at emission time. The phase shifting has brought the time records into close alignment but there are still differences due to variations in loading as the blade passes around the propeller disc. Read in conjunction with Figure 15, Figures 14 and 16 show the effect of the flow-field near the wing on the nearfield noise. The main difference in the time records is in the (phase shifted) position of the positive and negative peaks. The 0 and 180° records are quite closely aligned, as are the 90 and 270° signals but there is a pronounced difference between these two pairs of signals. Figure 14 gives some indication of why this could be so. Peaks in the time record are associated with maximum values of the source–observer velocity. It is the blade loading at such points that decides the strength of the peak radiated to the observer. Figure 16

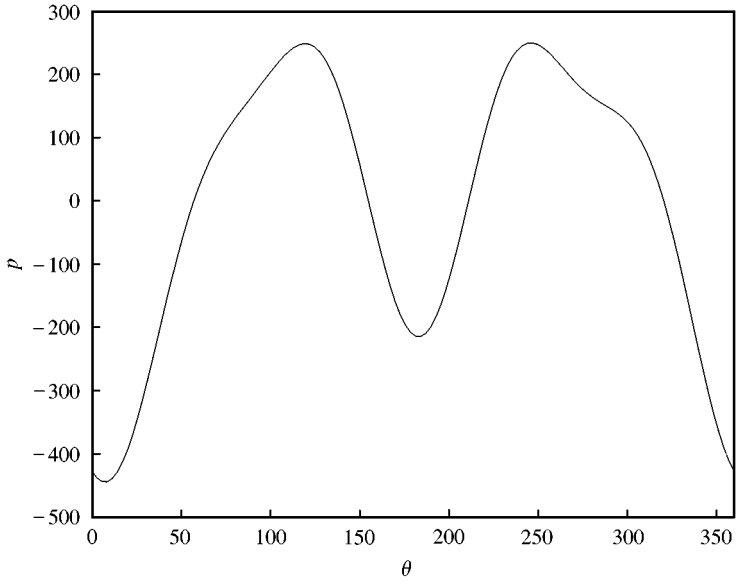

Figure 15. Blade loading variation near tip.

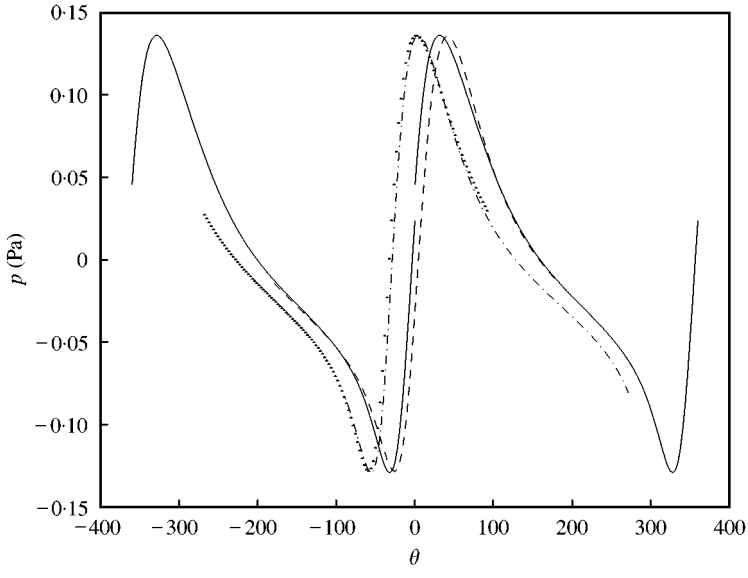

Figure 16. Phase shifted installed propeller time records, nearfield; (solid, 0° observer position; dash-dot, 90° observer position; dashed, 180° observer position; dotted, 270° observer position).

shows the loading at the tip section of the blade as a function of azimuth; there is a negative peak just after 0° and another 180° later, while there are positive peaks at 120 and 250°. These peaks occur with the blade just below the wing plane and appear to be associated with the blade entering or exiting the flow-field around the wing leading edge. At other positions, the blade, and especially the blade tip, is too far from the wing leading edge to be affected by it.

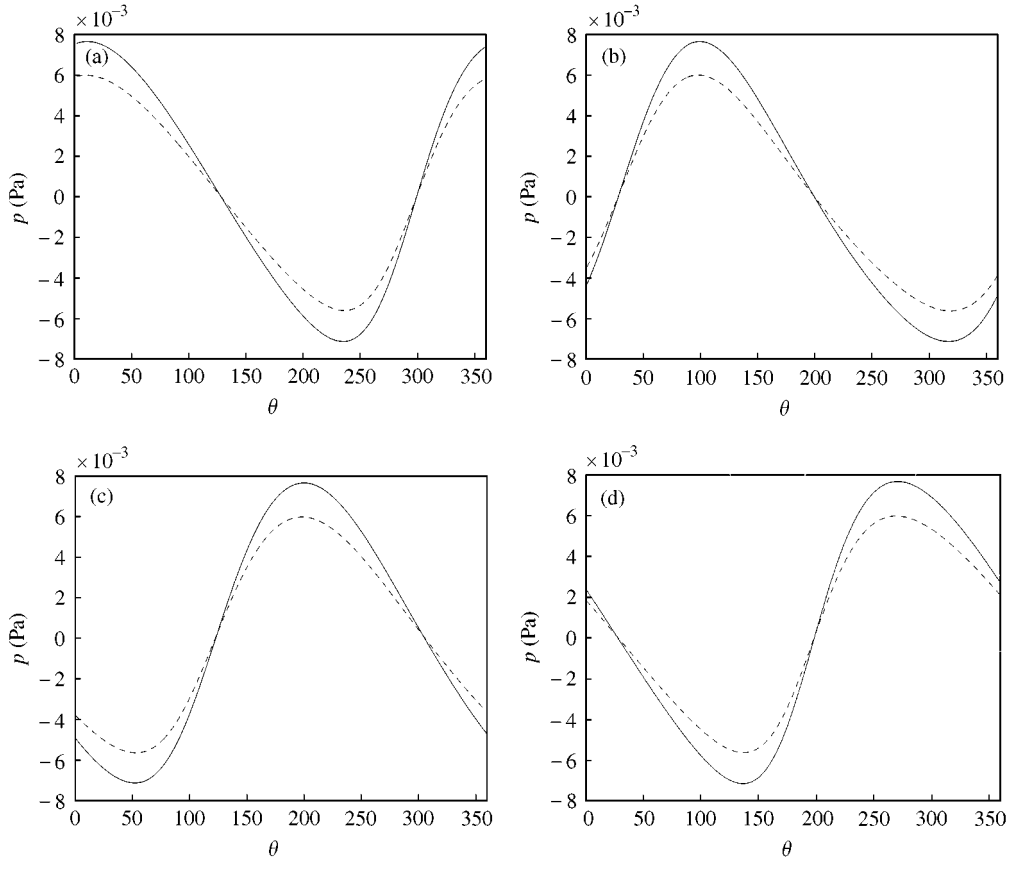

Figure 17. Farfield time records as a function of blade tip azimuth at emission time, isolated (solid) and installed (dashed) propeller. (a) 0° observer position; (b) 90° observer position; (c) 180° observer position; (d) 270° observer position.

In the far field, 10 blade radii from the propeller axis, the effect is rather different. Figure 17 shows the time records as a function of observer azimuth at 0, 90, 180 and 270° while Figure 18 shows the same data phase shifted and superimposed for comparison. The blade loading of Figure 15 is still appropriate to these plots. The farfield time records have rather less character than their nearfield counterparts with a smoother, more nearly sinusoidal form. When superimposed, Figure 18, they come more closely into alignment than in the nearfield case. This close alignment is due to the different nature of the farfield noise which is affected mostly by the changes in source–observer relative velocity, with very little effect of changes in source–observer distance. Thus, there is very little difference in the peak amplitudes of the farfield signals.

5. CONCLUSIONS

A method has been presented for the calculation of propeller aerodynamics and noise which allows the prediction of wing interference effects on the performance and acoustics of the system. The separate elements of the method have been previously validated and extend the reach of the techniques currently available.

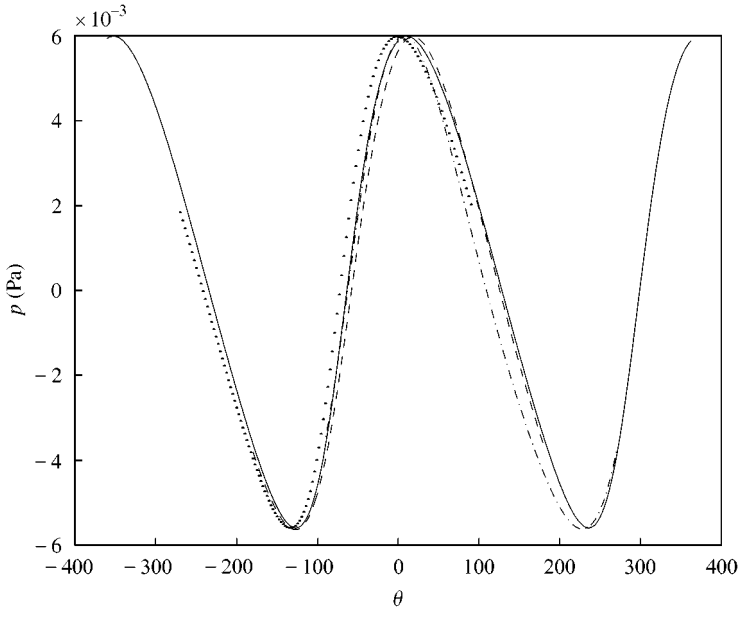

Figure 18. Phase shifted installed propeller time records, farfield; (solid, 0° observer position; dashed, 90° observer position; dash-dot, 180° observer position; dotted, 270° observer position).

The results presented show the installation effect of a wing on the propeller blade loading in terms of both the radiated acoustic field and the physics of the noise generation process (the aerodynamic conditions on the blade at the time of sound emission). The effect of the wing on the propeller acoustics appears to be to reduce the radiated noise. Since both the aerodynamic and the acoustic methods have proven accurate independently in the past, this effect is probably not due to numerical error. In a previous paper, studying only the aerodynamics, the propeller thrust coefficient (i.e., the blade loading) was found to vary above and below the isolated propeller value. The same effect here means that, although the propeller develops unsteady loading due to the wing flow-field, the net effect is to reduce slightly the radiated noise. This opens a useful line of inquiry to counterpoint currently available data for isolated propellers at incidence (e.g., the study of Hanson, [27]) where the effect of unsteady loading is almost invariably to increase the radiated noise.

Finally, we note perhaps a surprising result that the noise which is slightly reduced for an installed propeller is not unprecedented. In a paper containing measured noise on the fuselage of a twin-engine aircraft model [37], the noise on the fuselage was predicted numerically, including the effect of unsteady loading due to incidence, and corrected for installation effects by using a correlation obtained for flight effects on a full-size aircraft. For some of the data points, application of this correlation gives slightly lower sound levels than predicted by the numerical model (Figure 11 of reference [37]). Although these data are not directly comparable (they are taken for a higher speed propeller than that considered here) they do demonstrate that the effect of installation on a propeller need not always be to increase the noise.

ACKNOWLEDGMENTS

The present work was partially supported by the Italian Ministry of University and Scientific and Technological Research (MURST). Part of this work was conducted while the

second author was at the Department of Mechanical and Industrial Engineering of the Third University of Rome under an Italian-Irish bilateral agreement.

REFERENCES

1. E. J. H. LYNAM and H. A. WEBB 1919 *Aeronautical Research Committee Report* **624**. The emission of sound by airscrews.
2. M. J. LIGHTHILL 1952 *Proceedings of the Royal Society* (*A*) **211**, 564–587. On sound generated aerodynamically. Part 1. General theory.
3. J. E. FFOWCS WILLIAMS and D. L. HAWKINGS 1969 *Philosophical Transactions of Royal Society London* (*A*) **264**, 321–342. Sound generation by turbulence and surfaces in arbitrary motion.
4. F. FARASSAT 1981 *American Institute of Aeronautics and Astronautics Journal* **9**, 1122–1130. Linear acoustic formulas for calculation of rotating blade noise.
5. F. FARASSAT 1985 *Aerodynamics and Acoustics of Propellers*, *AGARD* CP-366 16. Theoretical analysis of linearized acoustics and aerodynamics of advanced supersonic propellers.
6. D. B. HANSON 1983 *American Institute of Aeronautics and Astronautics Journal* **21**, 881–888. Compressible helicoidal surface theory for propeller aerodynamics and noise.
7. R. M. ARDITO MARRETTA, G. DAVI, G. LOMBARDI and A. MILAZZO 1999 *Computers and Fluids* **8**, 923–950. Hybrid numerical technique for evaluating wing aerodynamic loading with propeller interference.
8. M. JUNGER and D. FEIT 1986 *Sound, Structures and Their Interaction*. Cambridge, U.S.A.: Massachusetts Institute of Technology Press.
9. J. M. GALLMAN, M. K. MYERS and F. FARASSAT 1991 *American Institute of Aeronautics and Astronautics Journal* **29**, 2038–2046. Boundary integral approach to the scattering of nonplanar acoustic waves by rigid bodies.
10. T. Q. WANG and S. ZHOU 1998 *Journal of Sound and Vibration* **209**, 317–328. Investigation on sound field model of propeller aircraft—the effect of rigid fuselage boundary.
11. T. Q. WANG and S. ZHOU 1998 *Journal of Sound and Vibration* **2**, 299–316. Investigation on sound field model of propeller aircraft—the effect of vibrating fuselage boundary.
12. M. H. DUNN and F. FARASSAT 1992 *American Institute of Aeronautics and Astronautics Journal* **30**, 1716–1723. High speed propeller noise prediction: a multidisciplinary approach.
13. S. E. WRIGHT 1969 *Journal of Sound and Vibration* **9**, 223–240. Sound radiation from a lifting rotor generated by asymmetric disk loading.
14. M. CARLEY 1997 *Ph.D. Thesis*, Trinity College, University of Dublin. Prediction of noise generated by a propeller in a flow.
15. M. CARLEY 1998 *Technical Report*. SCRUMPI: Simulation Code for Rotation of Unsteady Source Multibladed Propellers at Incidence. Dublin: Department of Mechanical Engineering, Trinity College.
16. J. Y. CHIARAMONTE, D. FAVIER, C. MARESCA and S. BENNECEUR 1996 *American Institute of Aeronautics and Astronautics Journal of Aircraft* **1**, 46–53. Aerodynamic interaction study of the propeller/wing different configurations.
17. D. WITKOWSKI, A. LEE and J. SULLIVAN 1989 *American Institute of Aeronautics and Astronautics Journal of Aircraft* **9**, 829–836. Aerodynamic interactions between propellers and wings.
18. J. CHO and M. H. WILLIAMS 1990 *American Institute of Aeronautics and Astronautics Journal of Aircraft* **3**, 196–203. Propeller–wing interaction using a frequency domain panel method.
19. A. ROTTGERMANN and S. WAGNER 1995 *Proceedings of ICES-IABEM'95 Symposium*, HI, U.S.A. Berlin: Springer-Verlag. *Computational Mechanics* **2**, 2915–2920. Compressible potential flow around a helicopter rotor.
20. F. CATALANO MARTINI 1995 *Proceedings of the 13th COBEM-CIDIM'95 Symposium, Belo Horizonte, Brazil*, available on CD Rom, (BKM editions, Belo Horizonte). The aerodynamic characteristics of a smooth wing at low Reynolds number under effect of a pusher propeller.
21. A. S. KINNAS and C. Y. HSIN 1992 *American Institute of Aeronautics and Astronautics Journal* **30**, 688–696. Boundary element method for the analysis of the unsteady flow around extreme propeller geometries.
22. A. GRABER and A. ROSEN 1987 *American Institute of Aeronautics and Astronautics Journal of Aircraft* **5**, 289–290. Velocities induced by semi-infinite helical vortex filaments.

23. H. YAMAGUCHI and N. BOSE 1994 *Proceedings of the Fourth International Offshore and Polar Engineering Conference*, *Osaka*, *Japan*, *I.S.O.P.E.* **3**, 539–544. Oscillating foils for marine propulsion.
24. N. BOSE 1995 *International Shipbuilding Progress* **432**, 281–294. Performance of chordwise flexible oscillating propulsors using a time-domain panel method.
25. R. H. G. MÜLLER, M. NSI MBA, E. AYMARD, D. FAVIER, E. BERTON and C. MARESCA 1996 *Experiments in Fluids* **3**, 161–169. Visualization and measurement of helicopter rotor flow with swept back tip shapes at hover flight using the "flow visualization gun" time line technique.
26. R. M. ARDITO MARRETTA, M. CARLEY, G. DAVI, G. LOMBARDI and A. MILAZZO 1999 *Computer Modeling and Simulation in Engineering* **4**, 104–116. Simulation model and computation of noise emission of an installed propeller.
27. D. B. HANSON 1995 *Proceedings of the Royal Society* (*A*) **449**, 315–328. Sound from a propeller at angle of attack: a new theoretical viewpoint.
28. R. M. ARDITO MARRETTA 1996 *American Institute of Aeronautics and Astronautics Journal of Aircraft* **5**, 919–923. Performance of a propeller embedded in the flowfield of a wing.
29. R. M. ARDITO MARRETTA, G. DAVI, G., LOMBARDI and A. MILAZZO 1997 *Computer Modeling and Simulation in Engineering* **2**, 304–321. Wing–propeller coupling simulation from tractor up to hover flight conditions.
30. D. B. HANSON and M. R. FINK 1979 *Journal of Sound and Vibration* **62**, 19–38. The importance of quadrupole sources in prediction of transonic tip speed propeller noise.
31. I. E. GARRICK and C. E. WATKINS 1953 *NACA Report* **1198**. A theoretical study of the effect of forward speed on the free-space sound-pressure field around propellers.
32. F. FARASSAT 1994 *NASA Technical Paper* **3428**. Introduction to generalized functions with applications in aerodynamics and aeroacoustics.
33. D. FAVIER and C. MARESCA 1984 *AGARD FDP on Aerodynamics and Acoustics of Propellers CP-366* **15**. Etude du sillage 3D d'une hélice aérienne quadripale.
34. D. FAVIER, M. NSI MBA, C. BARBI and C. MARESCA 1985 *Proceedings of the* 11*th European Rotorcraft Forum*, London, Vol. **21**, 493–511. A free-wake analysis for hovering rotors and advancing propellers.
35. D. FAVIER, A. ETTAOUIL and C. MARESCA 1989 *American Institute of Aeronautics and Astronautics Journal of Aircraft* **9**, 837–846. Numerical and experimental investigation of isolated propeller wakes in axial flight.
36. J. ŠULC, J. HOFR and L. BENDA 1982 *Journal of Sound and Vibration* **84**, 105–120. Exterior noise on the fuselage of light propeller driven aircraft in flight.
37. T. ZANDBERGEN, S. L. SARIN and R. P. DONNELLY 1984 *American Institute of Aeronautics and Astronautics/National Aeronautics and Space Administration Nineth Aeroacoustics Conference*, *Williamsburg*, *VA*, *USA*, *AIAA paper* 84-2367. Propeller noise measurements in DNW on the fuselage of a twin engine aircraft model.